1-1-2013

Enhancing superconducting properties of MgB2 pellets by addition of amorphous magnetic Ni-Co-B nanoparticles

Mislav Mustapic
University of Wollongong, mislav@uow.edu.au

Josip Horvat
University of Wollongong, jhorvat@uow.edu.au

Md Shahriar Hossain
University of Wollongong, shahriar@uow.edu.au

Zeljko Skoko
University of Zagreb

S X. Dou
University of Wollongong, shi@uow.edu.au

Enhancing superconducting properties of MgB2 pellets by addition of amorphous magnetic Ni-Co-B nanoparticles

Abstract

Amorphous magnetic Ni-Co-B nanoparticles with an average size of 5 nm were added to precursor powders of MgB2 superconductor. The preparation procedure for MgB2 pellets was optimized for obtaining the best critical current density (Jc) at elevated magnetic fields. Addition of Ni-Co-B decreases the Jc for heat treatment of precursor powders at 650 ° C. Heat treatments at 770 ° C and higher improve Jc at 20 and 5 K. This improvement occurs at both temperatures through the increase of the effective connectivity between MgB2 crystals. Vortex pinning was enhanced at 5 K, but not at 20 K. Ni-Co-B nanoparticles reacted with Mg in heat treatments above 730 ° C, forming Mg2Ni and MgCo2 nanoparticles. Ni-Co-B addition was associated with lower oxygen content in MgB2, indicating that reduction of MgO content is the mechanism for improvement of grain connectivity. Decomposition of magnetic Ni-Co-B nanoparticles results mostly in non-magnetic nanoparticles, so magnetic pinning did not occur in our samples.

Keywords

b, superconducting, enhancing, co, nanoparticles, ni, magnetic, amorphous, addition, pellets, mgb2, properties

Disciplines

Engineering | Physical Sciences and Mathematics

Publication Details

Mustapic, M., Horvat, J., Hossain, M., Skoko, Z. and Dou, S. X. (2013). Enhancing superconducting properties of MgB2 pellets by addition of amorphous magnetic Ni-Co-B nanoparticles. Superconductor Science and Technology, 26 (7), 1-9.

Enhancing superconducting properties of MgB_2 pellets by addition of amorphous magnetic Ni-Co-B nanoparticles

M Mustapić[1], J Horvat[1], M S Hossain[1], Ž Skoko[2] and S X Dou[1]

[1]Institute for Superconducting and Electronic Materials, AIIM, University of Wollongong, Squires Way, North Wollongong, NSW 2500, Australia

[2]Department of Physics, Faculty of Science, University of Zagreb, Bijenička c. 32, 10000 Zagreb, Croatia

Email: jhorvat@uow.edu.au

Abstract. Amorphous magnetic Ni-Co-B nanoparticles with average size of 5 nm were added to precursor powders of MgB_2 superconductor. Preparation procedure for MgB_2 pellets was optimized for obtaining the best critical current density (J_c) at elevated magnetic fields. Addition of Ni-Co-B decreases J_c for heat treatment of precursor powders at 650 °C. Heat treatments at 770 °C and higher improve J_c at 20 and 5 K. This improvement occurs at both temperatures through the increase of the effective connectivity between MgB_2 crystals. Vortex pinning was enhanced at 5 K, but not at 20 K. Ni-Co-B nanoparticles reacted with Mg in heat treatments above 730 °C, forming Mg_2Ni and $MgCo_2$ nanoparticles. Ni-Co-B addition was associated with lower oxygen content in MgB_2, indicating that reduction of MgO content is the mechanism for improvement of grain connectivity. Decomposition of magnetic Ni-Co-B nanoparticles results mostly in non-magnetic nanoparticles, therefore magnetic pining did not occur in our samples.

PACS: 74.70, 74.25

1. Introduction

Improvement of vortex pinning in MgB_2 has been one of the main activities in the development of this superconductor into a practical conductor. Numerous additions to MgB_2 were tried. Some of the most successful additions incorporate nanoparticles into MgB_2 precursor powder [1-8], which act as pinning centres either by themselves, or through products of their reaction with precursor powders. The mechanism of vortex pinning is typically the minimization of the vortex core energy as the volumes of the vortex core and pinning centre overlap [9]. However, if the nanoparticles incorporated into MgB_2 matrix are magnetic, additional pinning is possible through interaction between the magnetic moments of the vortex and nanoparticle [10-12]. Theoretical treatment has shown that the magnetic part of the pinning force between the vortex and magnetic nanoparticle has a range of London penetration depth [10], which is much larger than the range for the usual vortex core-type pinning, coherence length.

The possibility of long-range pinning by magnetic nanoparticles prompted research aimed at finding the most suitable nanoparticles for introduction of magnetic pinning into MgB_2 [13-19]. The idea of magnetic-type pinning in MgB_2 is still controversial. The reports on pinning by magnetic nanoparticles in MgB_2 are often conflicting and inconclusive. Unfortunately, reports showing the increase of pinning generally do not distinguish the core-type pinning from magnetic pinning in the investigated samples and therefore do not prove that the magnetic pinning was introduced in MgB_2.

This paper reports on the use of amorphous magnetic Ni-Co-B nanoparticles to improve J_c of MgB_2 at elevated magnetic fields [20]. Ni-Co-B nanoparticles were prepared by an improved method, making them smaller than what was tried so far with MgB_2, about 5 nm in diameter. Thus, they were expected to be good core-type pinning centres if incorporated into MgB_2 unit cell. Both Ni and Co contribute to magnetic moment of these nanoparticles, which can facilitate magnetic-type pinning. An independent study of Novosel et al. with Ni-Co-B nanoparticles 15-20 nm in diameter incorporated into MgB_2/Fe wires using a heat treatment at 650 °C was carried out in parallel to our work [21]. One major difference between our work and [21] is that we used quite different sample preparation techniques, much smaller Ni-Co-B nanoparticles and different sample characterization, leading to new insights into chemistry of heat treatment, grain connectivity and vortex pinning obtained by Ni-Co-B doping.

2. Experimental details

Nickel-cobalt-boron amorphous nanoparticles were synthesised by the chemical reduction of metallic salts. $Ni(NO_3)_2$ and $Co(NO_3)_2$ were dissolved in deionized water and reduced with the help of $NaBH_4$, which was previously dissolved in deionized water. The amount of all three chemicals corresponded to the nominal composition Ni-Co-B. The synthesis was performed in a closed system under argon atmosphere, and all solutions were bubbled with argon for two hours prior to the reaction. Ethylenediamine was added to maintain the reaction under alkaline pH

conditions (pH ≈ 8-10) and also catalyse the reaction. Reaction with this catalyst can provide yields of up to 90%. Sodium-dodecyl-sulphate was added as a surfactant to prevent agglomeration of nanoparticles. 90% of the obtained Ni-Co-B nanoparticles were of the size between 5 and 6 nm, as obtained from FESEM images. No agglomeration was observed. XRD analysis shows that the nanoparticles were amorphous, giving a very broad XRD peak between $35\ ° < 2\theta < 57\ °$ and a broad peak centred at 62 °. Measurements of the temperature dependence of magnetic moment show that the nanoparticles were in superparamagnetic state with blocking temperature of 90 K.

MgB_2 pellet samples were prepared using 99% pure amorphous boron powder with grain size of ~1 μm and 99% pure Mg powder with grain size ~3 μm. Ni-Co-B nanoparticles in concentration of 0, 1.25, 2.5 and 5 wt% were added to the stoichiometric precursor Mg + 2B powder. The powders were mixed dry, first Ni-Co-B nanoparticles and boron, and then magnesium was added, ground, and pressed with 10 tonnes press into 10 mm diameter pellets. Samples were enclosed in iron tubes and sintered at 650, 770, 850 and 950 °C for 30 min under high-purity argon gas with a heating rate of 5 °C min^{-1}. The resulting pellets were cut into small bar-shaped pieces with dimensions of $1 \times 2 \times 3\ mm^3$.

Nanostructure was studied using JEOL JSM7500FA scanning electron microscope (SEM), with a cold field emission gun. The microstructure was also studied by JEOL JSM-6400 scanning electron microscope. X-ray powder diffraction (XRD) was performed at room temperature using an automatic Philips diffractometer, model PW1820 (Cu-Kα radiation), in Bragg-Brentano geometry. XRD analysis was performed with the aid of FullProf package.

Magnetic measurements on nanoparticles were performed by Quantum Design MPMS-5T SQUID magnetometer and on MgB_2 samples by PPMS-9T extraction magnetometer. Magnetic hysteresis loops of MgB_2 samples were measured with the field parallel to the long axis of the sample. All samples were of the same size, to avoid size effects in our measurements [22, 23]. The magnetization was measured at 5 K and 20 K in a time-varying magnetic field with sweep rate 50 Oe s^{-1} and amplitude 9 T. Magnetic critical current density J_c was obtained by using the critical state model [24]: $J_c=20\Delta M/(a-a^2/(3b))$, where a and b are the lateral dimensions of the sample and ΔM is the thickness of the magnetic hysteresis loop. Differential thermal analysis (DTA) was performed on different combinations of Mg, B and Ni-Co-B powders, using Al_2O_3 pan. The powders were mixed in small quantities (200 mg), pressed to ensure good contact between grains in powder and heat flow from the sample was measured as the temperature increased up to 1000°C at a rate of 5K/min in protective Ar atmosphere.

The temperature dependence of electric resistance at a set of constant magnetic fields was measured for MgB_2 pellets in temperature range 30−300 K, using AC current of 1 mA and frequency 117 Hz. Electrical contacts were attached to the sample in four-probe geometry using a silver paste. The experiments were carried out in a Quantum Design PPMS-9T system, with sweep rate of temperature of 2 K/min.

3. Optimization of preparation procedure

The preparation procedure for precursor Ni-Co-B doped MgB_2 powders was optimized for highest value of J_c at elevated fields. The values of J_c obtained at 5 K and 5T, as well as at 20 K and 2 T were chosen for this optimization. These temperatures were chosen because they can provide information on the effect of π– and σ–gaps in vortex pinning [25-28] and because MgB_2 is likely to be used near these temperatures. Further, the values of the field were chosen so that the obtained values of J_c are not affected by artefacts of different screening lengths occurring in magnetic measurements of J_c [22, 23]. All samples were of the same size. We could not use J_c at the same field for 5 and 20 K, because the ranges of field for which reliable magnetic J_c can be obtained did not overlap for these two temperatures [22].

Figure 1a) shows that J_c at 5 T and 5 K decreased with the content of Ni-Co-B for samples heat treated at 650 °C. The same was obtained for J_c at 2 T and 20 K. For samples heat treated at higher temperatures, J_c measured at 5 and 20 K was better for samples with added Ni-Co-B nanoparticles than for pure MgB_2. The only exception was the sample with 1.25 wt% Ni-Co-B heat treated at 850 °C and measured at 20 K and 2 T (figure 1b). For all these samples, except the ones heat treated at 650 °C, J_c was the highest when 2.5 wt% of Ni-Co-B was added. Further, the highest J_c for samples with 2.5 wt% of Ni-Co-B was obtained for heat treatment at 850 °C (figure 1c).

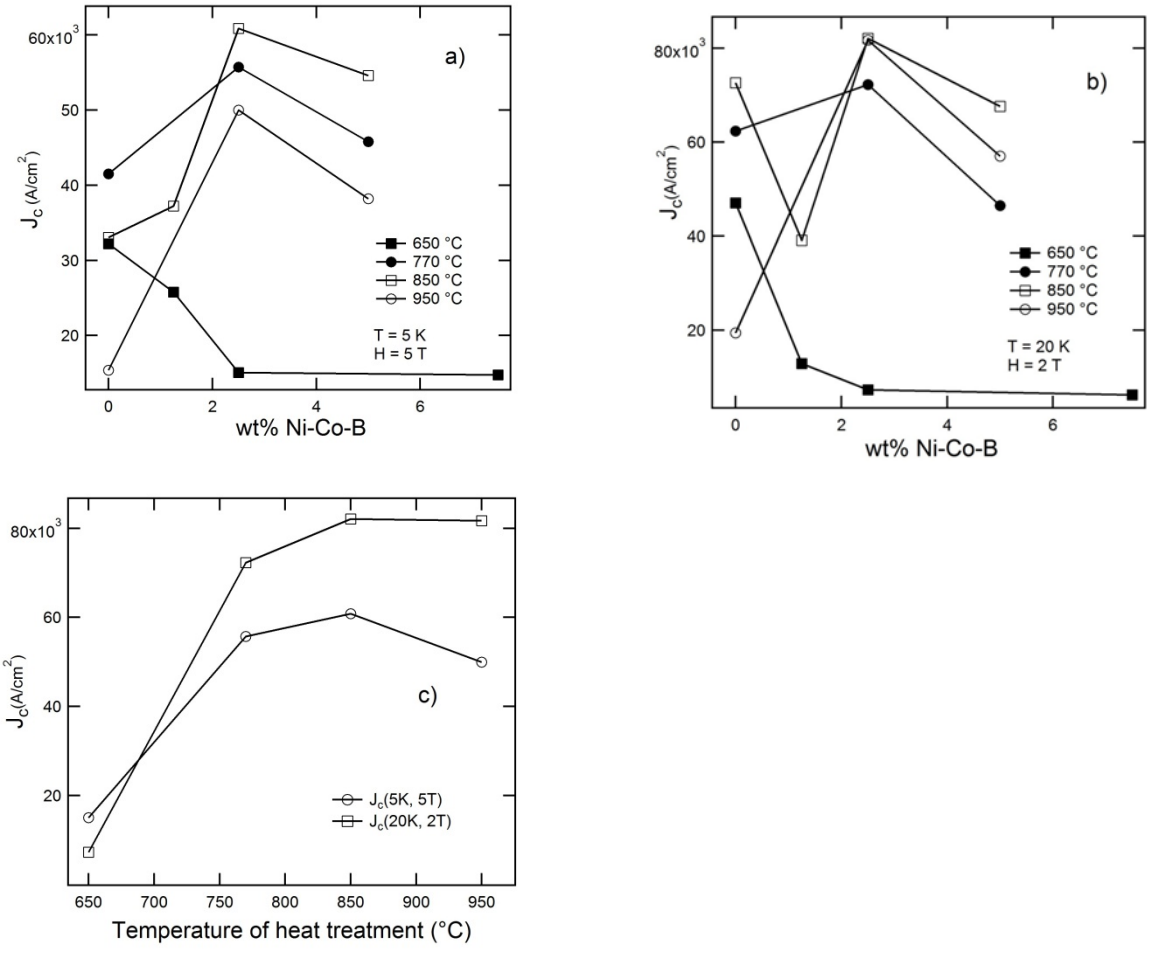

Figure 1: Dependence of J_c(5K, 5T) (figure a) and J_c(20K, 2T) (figure b) on the Ni-Co-B content in MgB_2 for different temperatures of heat treatment. Figure 1c shows the dependence of J_c(5K, 5T) and J_c(20K, 2T) on the temperature of heat treatment for samples containing 2.5 wt% of Ni-Co-B.

The field dependence of J_c for samples treated at 850 °C, with different concentration of Ni-Co-B nanoparticles, is shown in figure 2a. The artefacts in magnetic measurements of J_c, due to different screening lengths of superconducting currents in sample, occur outside the field range 1.5 T $< H <$ 3.5 T for 20 K and 4 T $< H <$ 8 T for 5 K, as described in [22]. Our discussion of $J_c(H)$ is therefore limited only to these fields, in which the experimental artefacts are absent. The best enhancement of $J_c(H)$ is obtained for 5K, where the $J_c(H)$ for different concentrations of Ni-Co-B is shifted to higher values of J_c as the concentration of Ni-Co-B increases to 2.5 wt%. In addition, $J_c(H)$ gets slightly less tilted with increasing Ni-Co-B content, indicating a weaker decrease of J_c with field as the Ni-Co-B concentration increases. This would indicate that addition of Ni-Co-B nanoparticles to precursor powders improves the connectivity between the MgB_2 crystallites and also increases the vortex pinning at 5 K. The $J_c(H)$ measured at 20 K (figure 2a) are parallel to each other, indicating only slight increase of grain connectivity with addition of Ni-Co-B nanoparticles, except for 1.25 wt% Ni-Co-B for which J_c decreases. Figure 2b shows the field dependence of J_c at 5K, for samples with 2.5 wt% of Ni-Co-B and heat treated at different temperatures. It is apparent that the heat treatment at 650 °C results in the lowest J_c for all fields. Heat treatment at 850°C gives the largest J_c.

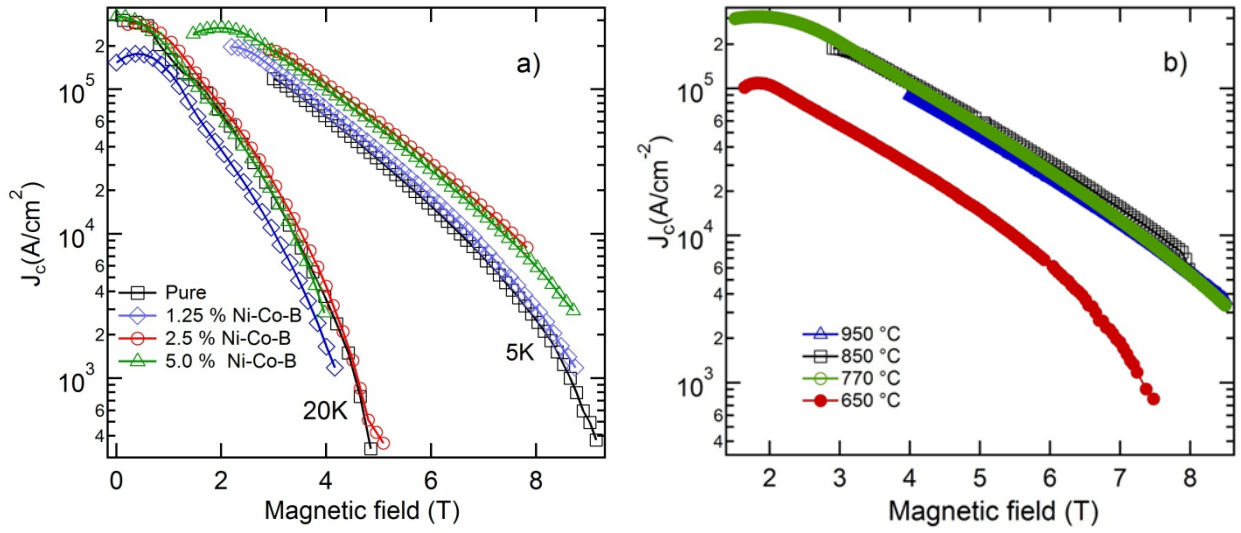

Figure 2: a) Field dependence of J_c for samples heat treated at 850 °C. b) Field dependence of J_c at 5K, for samples with 2.5 wt% of Ni-Co-B and heat treated at different temperatures.

To further clarify if vortex pinning increased with the Ni-Co-B addition, exponential decrease of J_c with H was assumed: $J_c=J_{c0}\exp(-H/H_0)$. The characteristic field H_0 was obtained from experimental $J_c(H)$ as $H_0 = -(d\ln(J_c)/dH)^{-1}$. Higher value of H_0 signifies a lower rate of the decrease of J_c with H and stronger vortex pinning. Figure 3 shows the field dependence of thus

defined H_0 at 5K, for the samples heat treated at 850 °C. The value of H_0 is not the same for all fields, as would be expected for the simple exponential form of $J_c(H)$. This occurs because the stretched exponential function fits $J_c(H)$ better than the simple exponential function [22]. The $\ln J_c$ vs H plots are not straight, but downward-curved (figure 2). Linear field dependence of H_0 is in agreement with the stretched exponential form of $J_c(H)$ and the deviation from linearity at highest fields in figure 3 is a consequence of artefacts in obtaining the J_c from magnetic hysteresis loops, as shown in [22]. However, the use of simple exponential $J_c(H)$ provides a more straightforward means of obtaining the rate of change of $\ln J_c$ with H, via a single parameter H_0. Figure 3 shows that 2.5 and 5 wt% Ni-Co-B samples have obviously larger value of H_0 than pure MgB_2 for all fields, while it seems to be just slightly larger for the 1.25 wt% Ni-Co-B sample. This shows that vortex pinning at 5K increases with Ni-Co-B addition for MgB_2 samples heat treated at 850 °C. The value of H_0 did not change with Ni-Co-B content at 20 K (inset to figure 3).

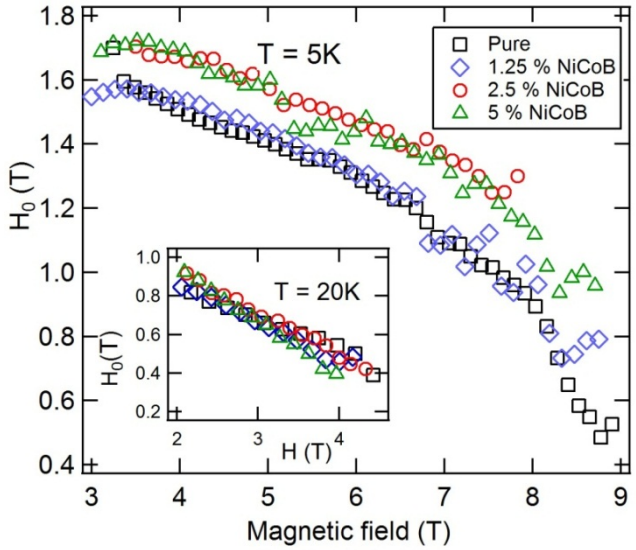

Figure 3: Field dependence of H_0 at 5K, for MgB_2 samples heat treated at 850 °C. Larger H_0 signifies a weaker decrease of J_c with field. Inset: Field dependence of H_0 at 20 K, for the same samples.

XRD patterns for MgB_2 samples with 2.5 wt% of Ni-Co-B nanoparticles, heat treated at 650, 770, 850 and 950 °C, are shown in figure 4. The samples with 2.5 wt% Ni-Co-B were chosen because this concentration gave the largest J_c. The main features in Fig 4 are well-defined patterns of MgB_2, with unreacted Mg and small amounts of MgO. Table 1 shows relative amounts of residual Mg, MgO and MgB_4 obtained from Rietveld analysis of all samples measured. The amount of MgO shows a decreasing trend with the amount of Ni-Co-B for heat treatment at 850 and 950 °C. This trend is less obvious for lower temperatures, where pure MgB_2 has the lowest amount of MgO. Residual Mg is present in samples heat treated at 650 °C due to low atomic diffusivity in solid-solid reaction [33]. This incomplete production of MgB_2 is responsible for low J_c for 650 °C treated samples (figure 2). MgB_4 phase occurs for heat treatment at 950 °C. Due to Mg evaporation, local boron-rich volumes can be formed in the sample, especially at high sintering temperatures. Thermodynamic analysis shows that MgB_2

coexists with MgB_4 in boron-rich volumes [29]. This MgB_4 is responsible for the observed decrease of grain connectivity and J_c for samples heat treated at 950 °C (figure 1).

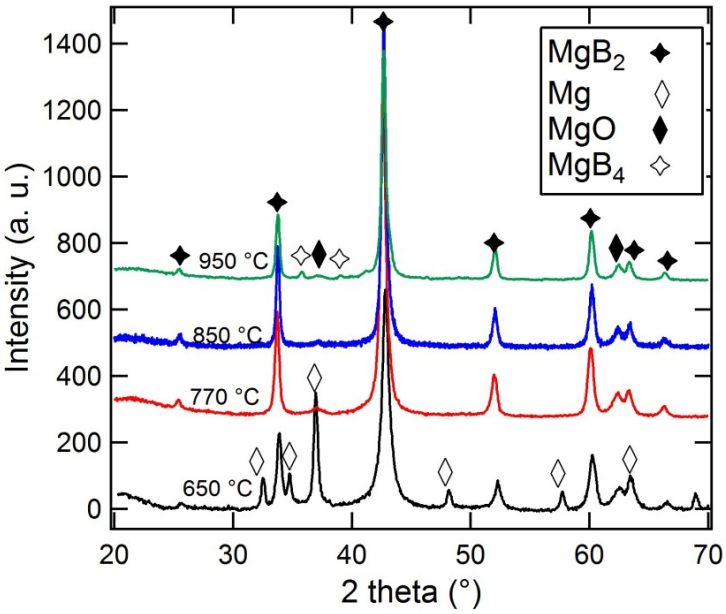

Figure 4: XRD patterns for 2.5% Ni-Co-B doped MgB_2 samples, heat treated at 650, 770, 850 and 950 °C.

Heat treatment temperature °C	Amount of added Ni-Co-B wt %	MgO %	Mg %	MgB_4 %
650	0.00	0.0	4.0	0.0
	1.25	20.4	8.8	0.0
	2.50	16.1	13.4	0.0
	7.50	5.4	5.9	0.0
770	0.00	12.2	0.2	0.0
	2.50	26.6	0.0	0.0
	5.00	17.1	0.0	0.0
850	0.00	16.2	0.0	0.0
	1.25	16.0	0.0	0.0
	2.50	12.2	0.0	0.0
	5.00	14.2	0.0	0.0
950	0.00	10.4	0.0	16.4
	2.50	15.2	0.0	9.4
	5.00	5.6	0.0	10.0

Table 1: Relative amounts of MgO, unreacted Mg and MgB_4, obtained by Rietveld analysis of the samples with different amounts of Ni-Co-B nanoparticles and prepared at different heat treatment temperatures.

SEM images of MgB_2 with 2.5 wt% of amorphous Ni-Co-B are shown in figures 5 a) and b) for heat treatment temperatures of 650 and 850 °C, respectively. The sample heat-treated at 650 °C has a large amount of ~ 10 nm-sized MgB_2 crystallites present. The sample treated at 850°C consists of somewhat larger crystallites, with ~10 nm flake-like crystallites still present. However, it is difficult to distinguish any significant difference between the two samples in terms of grain connectivity on the basis of SEM images. While larger MgB_2 grains of 850 °C treated sample would imply smaller density of interface surfaces in the sample, it is unclear how clean are these surfaces and how well they are connected. Further clues will be obtained from the EDS analysis.

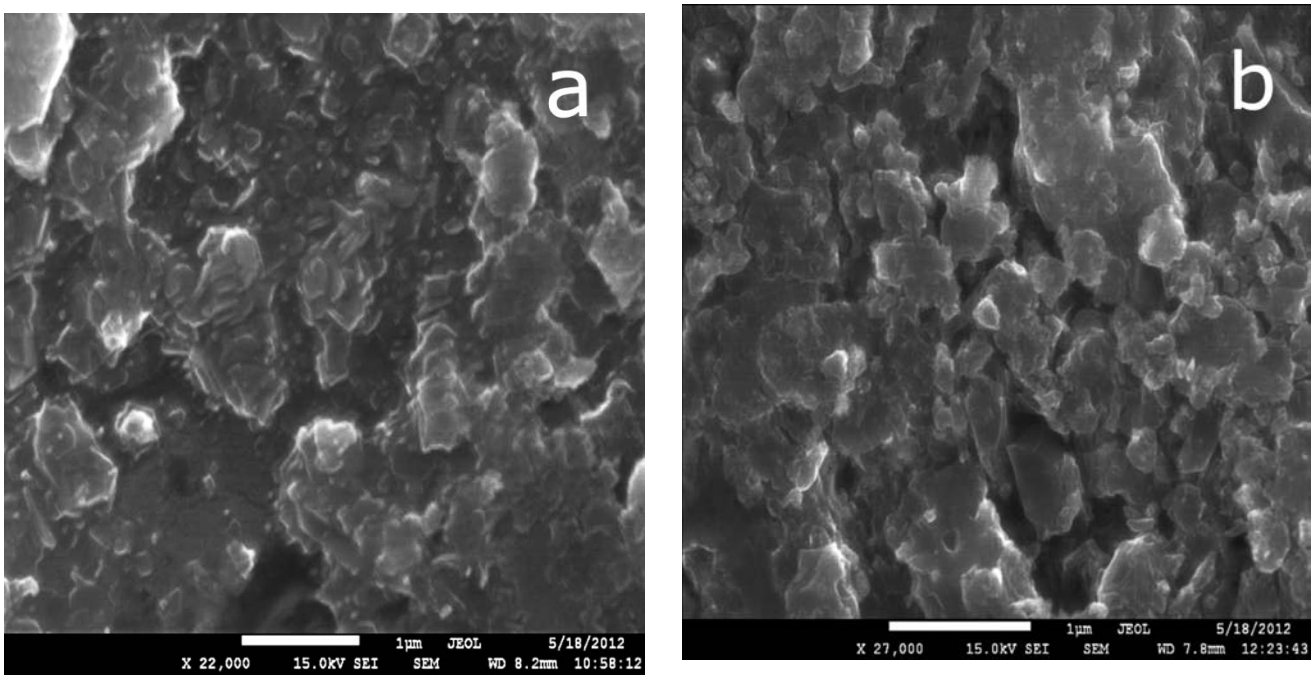

Figure 5: SEM images for 2.5 % Ni-Co-B doped MgB_2, heat treated at 650 (a) and 850 °C (b).

4. Effect of Ni-Co-B on grain connectivity and vortex pinning

Temperature dependence of resistivity, ρ, was measured for pure and 2.5 wt% Ni-Co-B sample heat treated at 850 °C, to obtain insight into the mechanisms of J_c improvement. The grain connectivity was analyzed using the Rowell's method [30], where the effective cross-sectional area fraction that contributes to supercurrent flow is: $A_F = \Delta\rho/(\rho_{300K}-\rho_{40K})$. Here, $\Delta\rho$ is the difference of the resistivities for perfectly connected MgB_2 sample at 300 and 40 K, 7.3 μΩcm, while ρ_{300K} and ρ_{40K} are the resistivities of the polycrystalline sample at 300 and 40 K, respectively. Our measurements gave A_F for pure and 2.5% Ni-Co-B sample as 0.22 and 0.32, respectively. Therefore, addition of Ni-Co-B nanoparticles to precursor powder improved the effective connectivity between the MgB_2 crystallites in our samples, resulting in higher J_c.

The residual resistance ratio (RRR) is the ratio of the resistance of the sample at 300 and 40 K. Assuming that the effective connectivity does not change with temperature above T_C, the differences in A_F between different samples are fractioned out and RRR provides information on the relative defect density in samples. Samples with smaller RRR have larger contribution of mostly temperature-independent defect mediated resistance to their resistivity. Therefore, samples with smaller RRR have larger defect densities in the MgB_2 crystallites, which would imply stronger vortex pinning. Our measurements gave RRR = 2.5 and 1.67 for pure and 2.5% Ni-Co-B sample, respectively. This implies that addition of Ni-Co-B nanoparticles to MgB_2 precursors most likely improves vortex pinning. However, because not all crystal defects contribute to vortex pinning, it is essential to confirm the improvement of vortex pinning by other means. The rate of the decrease of ln J_c with H shown in figure 3 has already shown that the pinning at 5 K increased with Ni-Co-B addition.

The vortex pinning can be further probed by measuring the temperature dependence of resistivity just below T_c. Vortices are thermally excited out of their pinning sites, contributing to a finite resistance of sample that follows the Arrhenius relationship: $R = R_0 \exp(-U/kT)$, where U is the effective pinning energy and kT is the thermal energy. Fitting only the lowermost experimental values of R to the Arrhenius relationship, the values of U can be obtained. These values of U are not directly related to pinning energy and J_c obtained from magnetic measurements, because of different voltage developed in the samples in magnetic and transport methods. Further, U obtained from the resistive transition is implicitly assumed to have negligible temperature dependence in the measured temperature range. However, analysis of resistive transition is still useful for comparing the pinning energies between different samples.

Our measurements of resistive transition near T_c for several different magnetic fields gave the effective pinning energies presented in figure 6. The sample containing 2.5 wt% of Ni-Co-B has clearly larger U than pure MgB_2 in fields up to 8 T, showing that Ni-Co-B addition improves vortex pinning.

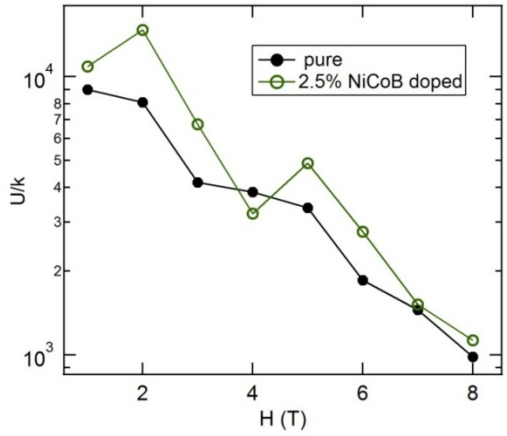

Figure 6: Pinning energies for pure and 2.5% Ni-Co-B doped MgB_2 samples heat treated at 850 °C, as obtained from the measurements of resistive transition at different magnetic fields.

These results may seem at odds with the measurements of $J_c(H)$ at 20 K, for which no pinning improvement was observed with Ni-Co-B addition (figure 2a). However the measurements of

magnetic hysteresis loops at 50 Oe/s and measurements of resistive transitions just below T_c probe different vortex dynamics. Further, there are different types of pinning centres in the samples, from grain boundaries, strain fields and crystal defects, to the pining centres introduced by Ni-Co-B addition. All these pinning centres contribute in a complex way to the total pinning potential [31]. Because of this, a direct comparison between the results based on magnetic and transport measurements is not appropriate. However, each of them separately can be used for comparison of vortex pinning between different samples.

5. Reaction of Ni-Co-B nanoparticles with precursor powder

The obtained measurements still do not demonstrate that the desirable magnetic pinning was obtained. To clarify this, further experiments were performed on samples containing large concentration (10 wt%) of Ni-Co-B, to help understand physics and chemistry of introducing Ni-Co-B nanoparticles into MgB_2.

Differential Thermal Analysis scans were performed to find out the chemical phase evolution during the heat treatment. Several different powder mixtures were used in DTA measurements: pure Ni-Co-B, Ni-Co-B with boron, Ni-Co-B with boron and magnesium in MgB_2 stoichiometric ratio and Mg + 2B (i.e. pure MgB_2) for comparison. DTA scan for pure Ni-Co-B nanoparticle powder showed that the nanoparticles were stable at these temperatures in protective Ar gas (figure 7). The scan of B + Ni-Co-B powder showed that Ni-Co-B did not react with boron up to 1000 °C. However, the DTA scan of Mg + 2B + Ni-Co-B powder showed an exothermic peak around 570 °C, a double exothermic peak between 730 and 850 °C and an endothermic peak at 650 °C (figure 7). The endothermic peak at 650 °C corresponds to melting of magnesium. The exothermic peak at 570 °C corresponds to creation of MgB_2 in solid-solid reaction [32]. The two merged peaks above 730 °C correspond to formation of new phases. These peaks hold the key to understanding the improvement of $J_c(H)$ with Ni-Co-B addition, because $J_c(H)$ started improving with the addition only when the temperature of heat treatment exceeded 770 °C (Figs. 1 and 2).

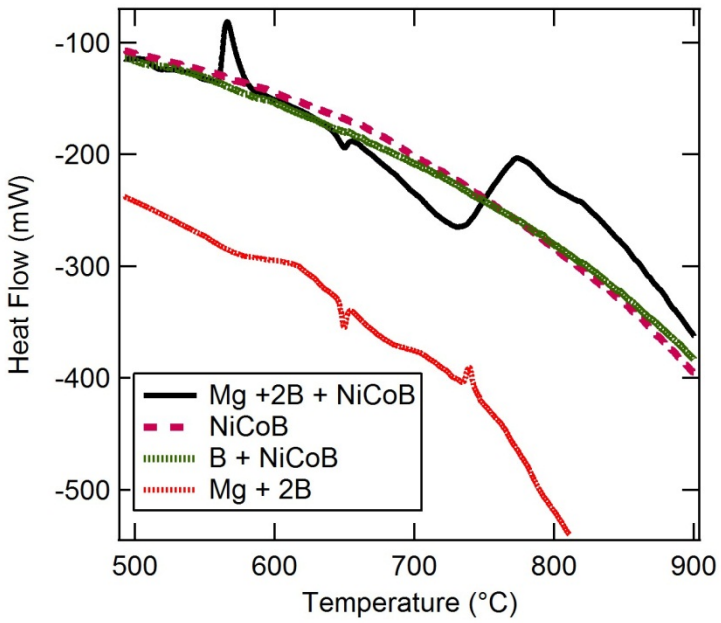

Figure 7: DTA scans for Mg + 2B, pure Ni-Co-B, B + 10wt% Ni-Co-B and Mg + 2B + 10 wt% Ni-Co-B powders.

DTA scan for pure MgB_2 has a broad exothermic peak between 570 and 630 °C, corresponding to creation of MgB_2 in solid-solid reaction (figure 7). There is an endothermic peak at 650 °C, due to melting of magnesium. A further broad exothermic peak around 700 °C and a sharp one at 730 °C are generally ascribed to creation of MgB_2 in solid-liquid reaction [33]. Production of MgB_2 in solid-solid reaction at low temperatures is spatially limited, due to low diffusion rate of atoms. Consequently, remaining Mg and B will react further after melting of Mg, producing additional DTA peaks. This is a complex process, involving re-arrangement of unreacted B and MgB_2 particles in molten Mg, reaction between molten Mg and residual boron, as well as melting of small MgB_2 grains in Mg and their re-precipitation on larger MgB_2 grains [33]. The exothermic peak at 730 °C is masked in Mg + 2B + Ni-Co-B powder by the larger peaks occurring because of reaction of Ni-Co-B with Mg. The broader MgB_2 creation peak at about 700 °C is still visible for Mg + 2B+ Ni-Co-B powder. This reaction of Ni-Co-B will be confirmed by magnetic measurements later in the paper. It is noticeable that the exothermic peak for Mg + 2B + Ni-Co-B powder at 570 °C is much larger than the corresponding peak for Mg + 2B powder. A possible explanation for this is that Ni-Co-B nanoparticles act as catalysts for production of MgB_2 from solid Mg and B powders. Similar mechanism was described by Zhao et al. [34] for Ni nanoparticles, which form a local eutectic liquid with Mg at 506 °C and thus promote a faster local formation of MgB_2 in the eutectic liquid phase. They also obtained an enhanced DTA peak below 600 °C with Ni nanoparticles, similar to our results (figure 7) and their Ni nanoparticles were of similar size to our Ni-Co-B nanoparticles (5 nm).

The DTA peaks for Mg + 2B + Ni-Co-B powder occurring between 730 and 850 °C will result in compounds involving Mg, Ni, Co and B. MgB_2 is one expected phase forming in reaction of Mg and B from Ni-Co-B, which will also form in the reaction of molten Mg with the remains of the micro-sized B powder at these temperatures. Phase diagrams of Mg-Ni system show that Mg_2Ni occurs as a stable phase at concentrations of Ni less than 35% [35-37]. For Mg-Co

system, there is only one stable compound, $MgCo_2$ [35-38]. Mg_2Co is not an equilibrium phase, however its low-yield production was reported in experiments where nanostructure and hydrogen atmosphere play an important role [35-38]. Therefore, Mg_2Ni and $MgCo_2$ are the phases expected to occur between 730 and 850 °C.

X-ray diffraction patterns of the Mg + 10 wt% Ni-Co-B samples heat treated at 650 and 850 °C are shown in figure 8. The peaks of Mg are clearly visible. Any difference between the two XRD traces should reveal the phases that form above 730 °C, as detected by DTA (figure 7). The position and magnitude of the peaks expected for Mg_2Ni and $MgCo_2$ [35, 39, 40] are also indicated in figure 8. If these phases are detectable by XRD, peaks around $2\theta = 21°$ and 45 ° should be seen for 850 °C treated sample but not for 650 °C treated sample. While there are small peaks at these angles, they appear for both samples. Therefore XRD analysis cannot confirm that the above phases formed, most likely because these phases were in the form of nanoparticles with poor crystallinity.

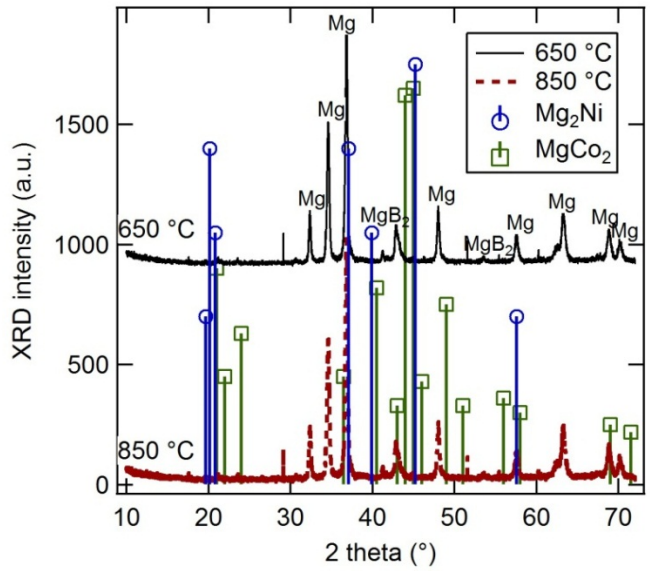

Figure 8: XRD patterns for Mg + 10wt% Ni-Co-B powders heat treated at 650 and 850 °C. The expected XRD peaks for Mg_2Ni and $MgCo_2$ are indicated for comparison [35, 39, 40].

To assess the distribution of chemical elements in the samples, Energy dispersive x-ray spectroscopy (EDS) analysis was performed over small areas of the samples, ranging from 100 x 100 nm^2 to 1 x 1 μm^2. For each of the areas, relative molar percentage of B, Mg, O, Ni and Co was obtained. While this method cannot provide an accurate percentage of the element distribution, it can serve as a rough guide. Figure 9a shows the molar percentage of Ni and Co in selected EDS windows against the magnesium content normalized to its stoichiometric percentage in MgB_2, for 2.5 wt% Ni-Co-B doped MgB_2 sample heat treated at 850 °C. For the values of x-axis in figure 9 smaller or larger than one, we probed the boron-rich or magnesium-rich area of MgB_2 sample, respectively. The measurements show that Ni and Co occur prevalently in the magnesium rich areas. The 2.5 wt% Ni-Co-B sample heat treated at 650 °C does not give such distribution of Ni and Co in regards to magnesium (inset to fig.9). Figure 9b shows the molar percentage of Ni and Co in selected EDS windows against the molar percentage

of oxygen. Large amounts on Ni and Co occur in the oxygen poor EDS windows. Therefore, Ni and Co oxides were not the prevalent phases formed in MgB_2 with added Ni-Co-B nanoparticles. All these results suggest that the compounds of Ni and Co with Mg are formed in MgB_2 with added 2.5 wt% Ni-Co-B, heat treated at 850 °C. This is in agreement with our DTA experiments with different powder mixtures (figure 7).

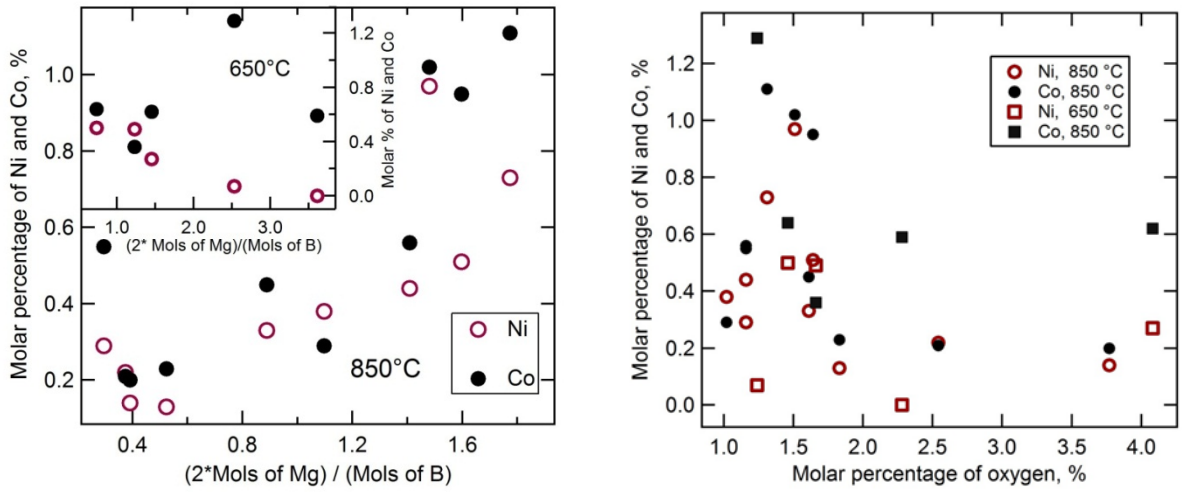

Figure 9: a) Molar percentage of Ni (open symbols) and Co (solid symbols) plotted against the relative amounts of Mg and B for 2.5 wt% Ni-Co-B sample heat treated at 850 °C, measured in several selected EDS windows. Inset: the same for the sample heat treated at 650 °C. b) Molar percentage of Ni (open symbols) and Co (solid symbols) plotted against the molar percentage of oxygen for 2.5 wt% Ni-Co-B sample heat treated at 650 and 850 °C.

Another interesting outcome of EDS analysis is the difference in the relative molar ratio of oxygen in samples, averaged over all measured EDS windows. For MgB_2 with added 2.5 wt% Ni-Co-B, the molar percentage of O was (2.1 ± 1.1) % and (1.8 ± 0.8) % for samples heat treated at 650 and 850 °C, respectively. For pure MgB_2, the molar percentage of O was (6.4 ± 0.9) % and (4.5 ± 1.4) % for samples heat treated at 650 and 850 °C, respectively. Despite large data scattering, due to difficulties in detecting these elements with EDS, this indicates that Ni-Co-B addition to MgB_2 results in a lower oxygen content. XRD analysis (table 1) shows that the amount of MgO generally decreases with the amount of Ni-Co-B for 850 and 950 °C heat treated samples, which is in agreement with EDS data. However, for heat treatment at 650 and 770 °C, pure MgB_2 has lower MgO content, according to XRD data (table 1). The improvement of the observed grain connectivity with Ni-Co-B addition could have occurred through hindrance of MgO formation on MgB_2 grain boundaries by Ni-Co-B during the heat treatment. Ni and Co may compete for Mg with oxygen, creating Mg_2Ni and $MgCo_2$ instead of MgO. In the same time, Mg_2Ni and $MgCo_2$ nanoparticles formed at higher temperatures result in increased vortex pinning.

Measurements of room-temperature magnetization curves for Mg + 10 wt% Ni-Co-B powders before and after the heat treatment at 850 °C (figure 10) gave insightful information regarding the type of vortex pinning introduced into MgB_2 by Ni-Co-B addition. The magnetization curve before heat treatment is typical for superparamagnetic system, giving the magnetic moment at 4 T and 300 K of 2.9 Am^2/kg. After the heat treatment at 850 °C, the magnetic moment at 4 T

decreased to 0.045 Am^2/kg, which is a 64-fold decrease. This shows that the reaction between Ni-Co-B nanoparticles and Mg gives mostly non-magnetic phases. Mg_2Ni is paramagnetic [41] and does not contribute substantially to the observed magnetic moment measured after the heat treatment. The only stable compound in Mg-Co system is $MgCo_2$ and it is a ferromagnet with Curie temperature of 321 K [36, 39, 42]. It undergoes antiferromagnetic transition at 45 K. It is possible that the low magnetic moment observed after the heat treatment in figure 10 is due to superparamagnetic nature of the resulting $MgCo_2$ nanoparticles and interference of the surface effects with their magnetic ordering. The temperature dependence of magnetic moment for $MgCo_2$ shows that its magnetic moment at 300 K is 55-60% of its moment below 40 K [41]. Assuming that the whole magnetic moment measured after the heat treatment is due to $MgCo_2$, the magnetic moment of the nanoparticles below 40 K would decrease at least 35 times by the heat treatmnet. Therefore, Ni-Co-B addition is very unlikely to produce the magnetic pinning, because the resulting phases are essentially non-magnetic.

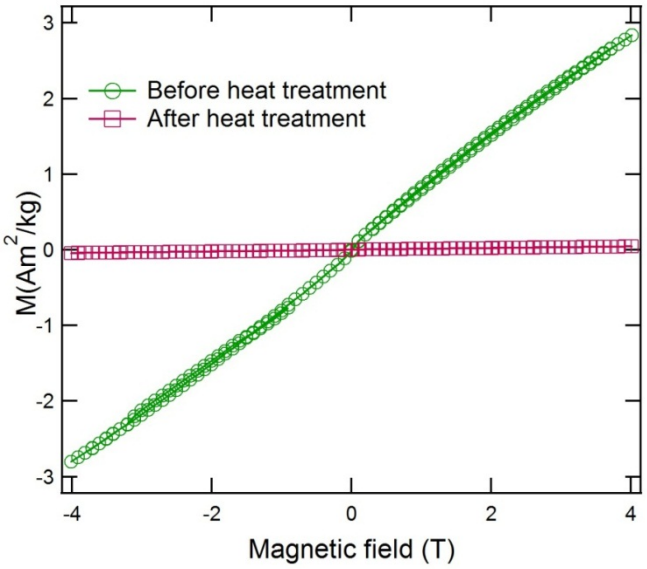

Figure 10: Magnetization curves measured at 300 K for Mg + 10 wt% Ni-Co-B powders before and after heat treatment at 850 °C.

6.Conclusions

Addition of magnetic Ni-Co-B nanoparticles to MgB_2 results in improvement of grain connectivity and vortex pinning when precursor powders are heat treated above 730 °C. The best performance of J_c in magnetic field is obtained for 2.5 wt% Ni-Co-B addition and heat treatment at 850 °C. Ni-Co-B nanoparticles react with Mg, creating Mg_2Ni and $MgCo_2$ nanoparticles. The resulting nanoparticles improve the vortex pinning. Because the magnetic moment of Ni-Co-B nanoparticles is reduced to almost zero in their reaction with Mg through 850 °C heat treatment, the resulting nanoparticles do not contribute to magnetic-type pinning. Grain connectivity improvement by Ni-Co-B doping is associated with a decrease of oxygen content in the samples. Most likely mechanism for improvement of connectivity is competition for Mg between Ni/Co and MgO at grain boundaries.

Acknowledgments

The lead author (M M) was recipient of University of Wollongong PhD scholarship for the duration of the work presented in this paper. This work builds up on the outcomes of a project UKF 1B 01/07, which was supported through Unity Through Knowledge Fund, designed by Croatian government, represented by the Ministry of Science, Education and Sport. The authors acknowledge the use of facilities and assistance of Mr Darren Attard and Tony Romeo at University of Wollongong Electron Microscopy Centre. Help of Dr Germanas Peleckis at ISEM is thankfully acknowledged.

References:

[1] Avdeev M, Jorgensen J D, Ribeiro R A, Bud'ko S L and Canfield P C 2003 Physica C 301.
[2] Yeoh W K, Kim J H, Horvat J, Xu X, Qin M J, Dou S X, Jiang C H, Nakatane T, Kumakura H and Munroe P 2006 Supercond. Sci. Technol. **19** 596.
[3] Takenobu T, Ito T, Chi D H, Prassides K and Iwasa Y 2001 Phys. Rev. B **64** 1345131.
[4] Wei J, Li Y, Xu C, Wei B and Wu D 2003 Mater. Chem. Phys. **78** 785.
[5] Ma Y, Zhang X, Nishijima G, Watanabe K, Awaji S and Bai X 2006 Appl. Phys. Lett. **88** 07250.
[6] Dou S X, Soltanian S, Horvat J, Wang X L, Zhou S H, Ionescu M, Liu H. K., Munroe P R and Tomsic M 2002 Appl. Phys. Lett. **81** 3419.
[7] Fujii H, Togano K and Kumakura H 2003 Supercond. Sci. Technol. **16** 432.
[8] Ma Y, Kumakura H, Matsumoto A, Hatakeyama H and Togano K 2003 Supercond. Sci. Technol. **16** 852.
[9] Cooley L D and Grishin A M 1995 Phys. Rev. Lett. **74** 2788.
[10] Snezhko A, Prozorov T and Prozorov R 2005 Phys. Rev. B **71** 024527.
[11] Milosevic M V, Yampolskii S V and Peeters F M 2002 Phys. Rev. B **66** 174519.
[12] Lyuksutov I F and Pokrovsky Y 1998 Phys. Rev. Lett. **81** 2344.
[13] Prozorov T, Prozorov N, Snezhko A ans Suslick K S 2003 Appl. Phys. Lett. **83** 2019.
[14] Chen S K, Wei M and MacManus-Driscoll 2006 Appl. Phys. Lett. **88** 192512.
[15] Cheng C and Zhao Y 2006 Appl. Phys. Lett. **89** 252501.
[16] Dou S X, Soltanian S, Zhao Y, Getin E, Chen Z, Shcherbakova O and Horvat J 2005 Supercond. Sci. Technol. **18** 710.
[17] Novosel N, Galic S, Pajic D, Skoko Z, Loncarek I, Mustapic M, Zadro K and Babic E 2012 Supercond. Sci. Technol **25** 095018.
[18] Awana V P S, Isobe M, Singh K P, Takayama-Muromachi E and Kishan H 2006 Supercond. Sci. Technol. **19** 551.
[19] Kuroda T, Nakane T, Uematsu H and Kumakura K 2006 Supercond. Sci. Technol. **19** 1152.
[20] E. Babić, University of Zagreb, suggested the use of Ni-Co-B nanoparticles.
[21] Novosel N, Galić S, Pajić D, Skoko Ž, Lončarek I, Mustapić M, Zadro K and Babić E 2013, manuscript submitted.
[22] Horvat J, Soltanian S, Pan A V and Wang X L 2004 J. Appl. Phys. **96** 4342.
[23] Horvat J, Soltanian S, Wang X L and Dou S X 2004 Appl. Phys. Lett. **84** 3109.
[24] Bean C P 1964 Rev. Mod. Phys. **36** 31.
[25] Bouquet F,Wang Y, Sheikin I, Plackowsky T, Junod A, Lee S and Tajima S 2002 Phys. Rev. Lett. **89** 257001.
[26] Iavarone M et al., 2002 Phys. Rev. Lett. **89** 1870021.
[27] Schmidt H, Zasadzinsky J E, Gray K E and Hinks D G 2002 Phys. Rev. Lett. **88** 1270021.
[28] Gurevich A et al. 2004 Supercond. Sci. Technol. **17** 278.
[29] Liu Z K, Schlom D G, Li Q and Shi X X 2001 Appl. Phys. Lett. **78** 3678.
[30] Rowell J M 2003 Supercond. Sci. Technol. **16** R17.
[31] Blatter G, Feigel'man M V, Geshkenbein V B, Larkin A I and Vinokur V M 1994 Rev. Mod. Phys. **66** 1125.
[32] Kühberger M and Gritzner G 2002 Physica C **370** 39.
[33]Liu Y C, Shi Q Z, Zhao Q and Ma Z Q 2007 J. Mater. Sci.: Mater. Electron **18** 855.
[34] Zhao Q, Liu Y, Zhao N, Penner S and Ma Z 2011 IEEE Transactions on Nanotechnology **10** 331
[35] Aizawa T, Hasehira K and Nishimura C 2003 Materials Transactions **44** 601.
[36] Shao H, Liu T, Wang Y, Hairuo X and Li X 2008 Journal of Alloys and Compounds **465** 527.
[37] Hanawalt J D and Nelson C E 1942 Trans. AIME **147** 273.
[38] Norek M et al. 2011 International Journal of Hydrogen Energy **36** 10760.
[39] Tatsuhiko A, Hasehira K-I, Nishimura C 2003 Materials Transactions **44** 601 .
[40] Chiba M, Hotta H, Nobuki T, Sotoma A and Kuji T 2007 Journal of Magnetism and Magnetic Materials **316** e454.
[41] Buschow K H J 1975 Solid State Comunications **17** 891.
[42] Kirkpatrick E M, Leslie-Pelecky D, Kim S-H and Rieke R D 1999 J. Appl. Phys. **85** 5375